Title: **Hydrogen Embrittlement of Automotive Advanced High-Strength Steels**

Authors: **G. Lovicu, M. Bottazzi, F. D'Aiuto, M. De Sanctis, A. Dimatteo, C. Santus, R. Valentini**

DOI Link: https://doi.org/10.1007/s11661-012-1280-8

HYDROGEN EMBRITTLEMENT OF AUTOMOTIVE ADVANCED HIGH STRENGTH STEELS

G. LOVICU[1]*, M. Bottazzi[2], F. D'Aiuto[2], M. De Sanctis[1], A. Dimatteo[1], C. Santus[3], R. Valentini[1]

[1]: *Dipartimento di Ingegneria Chimica, Chimica Industriale e Scienza dei Materiali - Università di Pisa, Italy*
[2]: *Centro Ricerche Fiat Scpa, Orbassano (TO), Italy*
[3]: *Dipartimento di Ingegneria Meccanica, Nucleare e della Produzione - Università di Pisa, Italy*

*: corresponding author.
Dipartimento di Ingegneria Chimica, Chimica Industriale e Scienza dei Materiali – Università di Pisa, Largo Lucio Lazzarino, 2 – 56126 Pisa – Italy
Tel: +39 050 2217860
Fax: +39 050 2217861
e-mail: g.lovicu@ing.unipi.it

KEYWORDS: AHSS, Martensitic steels, TRIP steel, Hot Stamping steel, Hydrogen Embrittlement, SSRT

ABSTRACT

Advanced High Strength Steels (AHSS) have a better combination between strength and ductility than conventional HSS and higher crash resistances are obtained in concomitance with weight reduction of car structural components. These steels have been developed in last decades and their use is rapidly increasing. Notwithstanding, some their important features have to be still understood and studied in order to completely characterize their service behavior. In particular, the high mechanical resistance of AHSS makes hydrogen related problems a great concern for this steel grades. This paper investigates the hydrogen embrittlement (HE) of four AHSS steels. The behavior of one TRIP, two martensitic with different strength levels and one hot stamping steels have been studied using Slow Strain Rate Tensile (SSRT) tests on electrochemically hydrogenated notched samples. The embrittlement susceptibility of these AHSS steels has been correlated mainly to their strength level and to their microstructural features. Finally, the hydrogen critical concentrations for HE, established by SSRT tests, have been compared to Hydrogen contents absorbed during the painting process of Body In White (BIW) structure, experimentally determined during a real cycle in an industrial plant.

I. INTRODUCTION

In last decades the development of new classes of high strength steels allowed to increase both resistance and toughness properties in respect to conventional high strength autobody steels. The transformation hardened steels (the so-called Advanced High Strength Steels) along with High Manganese Austenitic Steels are examples of new recently developed classes [1-4].
In conventional steels, more traditional hardening methods are used, such as solid solution, grain refinement or precipitation, whereas in AHSS less conventional ones, based on phase transformations, are applied. These methods allow to obtain complex microstructures, where mechanical properties of transformed phases are, to some extent, merged. Main classes are: Dual

Phase, TRIP, Martensitic, Complex Phase steels, and others. They differ in terms of type and volume fraction of microstructural constituents.
DP steels have a ferrite-martensite mixed microstructure [5], with a martensite volume fraction ranging from 20 to more than 75 % in respect to the steel grade. Typical tensile strength of DP steels are between 450 and 1100 MPa, and elongation between 10 and 25 %. The microstructure of TRIP steels consist of a ferritic matrix with dispersed islands of hard phase (bainite and/or martensite) and retained austenite [5]. During straining the metastable austenitic phase transforms into martensite (TRIP effect) increasing both strength and ductility. Between steels belonging to AHSS, the martensitic steels have the highest strength levels. Two main groups could be highlighted, the cold rolled martensitic steels for cold forming and the boron containing steels optimized for hot stamping. Typical tensile strength of martensitic steels can lie between 1000 and 1500 MPa. Despite of their limited elongation and high springback effect related to their high grades, cold rolled steels have having a great developing thank to their lower cost in respect to hot stamping components of similar strength. On the contrary, the Hot Stamping process permits to obtain high strength components with low residual stresses and more homogeneous microstructure, but with higher costs.
Generally, increasing the mechanical resistance of steels, also their hydrogen embrittlement susceptibility increases [6,8]. This is a general behaviour in steels belonging to the same class[8], although some researchers stress the role of all the parameters that influence the hydrogen embrittlment susceptibility, such as microstructures, trapping state, deformation state and also strength [9].
Hydrogen degradation could represent one of the main limit to the use of Advanced High Strength Steels. In steel, hydrogen can derive from production process, product assembling and finishing, or from service environment exposure. If hydrogen content reaches a critical value inside the steel, it can induce a strong reduction of mechanical properties, particularly strength and ductility. In case of conventional quench and tempered steels with UTS of about 1500 MPa, the critical value to induce hydrogen embrittlement can be much less than 1 wppm (see, for example [8]). Since the most part of car body components are produced by cold forming techniques that can induce high residual stresses, the effect of very little quantities of hydrogen can be catastrophic.
Although some experimental studies have been carried out on hydrogen embrittlement of AHSS [10-14], much work is still needed. In particular, the hydrogen effect on multiphase steels should be better related to peculiar microstructural features of steels. Above all, when an austenitic phase is also present, such as for TRIP steels, the effect of huge differences on transport and solubility properties of hydrogen within the austenite and the ferritic/martensitic matrix, as well the austenite tendency to transform to martensite during straining and/or during hydrogen charging, are all aspect of the problem which need to be thoroughly investigated.
One of the main experimental techniques used to analyze the hydrogen effect on mechanical properties of steels is SSRT test [15], i.e. a tensile test performed at slow strain rate in order to enhance the embrittlement effect of hydrogen. The hydrogen embrittlement mechanism is governed by local hydrogen transport within the steels. The high stressed areas (with a non-zero hydrostatic component) in the sample are subject to a lattice distortion able to increase the local hydrogen solubility and thus to generate a chemical potential gradient that can act as driving force for the hydrogen diffusion. Thus, areas with higher residual stresses not only are those subjected to higher stress level, but are also richer in hydrogen, dramatically increasing the failure susceptibility.
This paper analyses the hydrogen embrittlement behavior of four different AHSS by means of SSRT tests on electrochemically charged notched tensile samples. Obtained results, along with the fractografic studies of post tensile samples, have been deeply investigated in terms of their microstructural and mechanical features. Finally in order to compare the critical hydrogen concentrations determined by SSRT tests with the quantity of hydrogen absorbed in real conditions, particular attention have been put on the pre-treatment of painting process. As a matter of fact, phosphatizing, electrodeposition paint (EDP) processes could be responsible for some hydrogen

absorption [16]. The hydrogen concentration absorbed from different tested steels has been measured using the Barnacle Electrode method after exposition of steel specimens to a real industrial process.

II. MATERIALS AND EXPERIMENTAL METHODS

A. Materials

Four different commercial AHSS have been selected in order to investigate their hydrogen embrittlement susceptibility. In particular, one Hot Stamping, two martensitic and one TRIP steels have been analyzed. All steels have been received in their commercial coating conditions. Hot Stamping steel has been received in quenched condition, using the same temperature and cooling rate as for the real industrial hot stamping process.
Table 1 shows the chemical compositions along with the thickness and the coating characteristics of each studied steel.
In order to analyze their microstructures, each steel has been polished and then etched employing appropriate reagents depending on the expected microstructures. Nital reagent has been used for Hot Stamping and Martensitic steels, while Le Pera etchant has been used to highlight the complex microstructure of TRIP 800 steel.

B. Mechanical tests

Preliminary mechanical tests have been performed on as-received smooth tensile samples using a MTS[1] 100kN tensile machine, in order to measure the mechanical properties of as-received steels.

C. SSRT

Notched tensile samples, having the geometry and dimensions shown in Fig.1, have been used to carried out SSRT tests. The presence of a notch permits to obtain an hydrostatic stress state in its proximity, thus increasing the embrittling effect of hydrogen. Before hydrogenation, the sample surface had been prepared by removing the coating layer using SiC paper up to 600 grit.
Different electrochemical conditions have been used in order to obtain hydrogen contents ranging in a wide interval able to include the embrittlement of materials. Aqueous solutions containing NaOH (0,1 M), H_2SO_4 (0,1 N and 1 N) have been used, with addition of different recombination poisons, (As_2O_3, $NaAsO_2$). The cathodic current densities typically ranged from 1 to 50 mA/cm^2. Electrochemical charging time have been chosen in respect of saturation time of each steel, depending on specimen thickness and hydrogen diffusion coefficient [17], the latter measured by a Devanathan-Stackurski electrochemical permeation experiment [18].
Coupons of the same steel have been hydrogenated contemporary to the tensile samples to have witness specimens in order to measure the absorbed hydrogen content before tensile tests. Hydrogen concentration has been measured using a LECO[2] DH603 hydrogen determinator, based on hot extraction method.
SSRT tests have been performed following the ASTM G129 – 00 standard test method [19], using a strain rate of about $4 \cdot 10^{-5}\ s^{-1}$.
After SSRT tests one half of each fractured sample has been used for fractographic analysis, while the other half has been used to measure the post tensile hydrogen concentration by using the LECO DH603.

D. Hydrogen absorbed during painting process

Hydrogen uptake in autobody components may result from assembling and/or finishing processes. Because of the steel sheet thinness, no residual hydrogen is expected from the steel production process. Therefore, in this context, the painting process could represent its main source, as a

[1] MTS is a trademark of MTS Systems Corporation, Eden Prairie, MN.
[2] LECO is a trademark of the LECO Corporation, St. Joseph, MI.

consequence of the cathodic reactions in water solution that takes place in phoshatizing and electrophoresis stages [16]. During these reactions, atomic hydrogen can form on the steel surface. The main part of the hydrogen generated on steel surface recombines to form gaseous hydrogen, but some hydrogen can be absorbed and diffuse into the steel.
Some samples of the tested steels have been prepared and connected in a commercial Body In White structure in order to test the real cycle conditions. Tests have been performed in an industrial plant, during an usual production cycle. The main pre-treatment process parameters are summarized in Table 2. Three steps of the coating process have been analyzed: phosphatizing, Electro Deposition Paint (EDP) and the final curing stages.
After each step, three coupons of each steel have been extracted and stored in dry ice or liquid nitrogen until its hydrogen content have been measured in the laboratory.
For each sample two different conditions of coating layer have been analyzed: the undamaged state and the case of scratches presence in the protective layer. The latter condition was chosen in order to simulate the effect of galvanic coupling between the protective layer and the underlying metal.
The measurement of superficial absorbed hydrogen has been done by the Barnacle Electrode Method [20], following the ASTM F1113 standard test method [21]. The registered current output had been preliminary correlated to the hydrogen content using uniformly charged samples, whose hydrogen concentration had been measured using hot extraction method (using a LECO DH603).

E. Fractographic analysis

The post-tensile fractographic analysis have been performed using a JEOL[3] 5600LV Scanning Electron Microscope (SEM), interfaced with a X-ray spectrometer (EDS). The aim of these observations has been to highlight the correlation between the hydrogen concentration and the fracture modalities of each analyzed steel.

III. RESULTS

A. Microstructural investigation

Fig.2 shows the optical micrographs of tested steels. Hot stamping and Martensitic steels have a martensitic microstructure. TRIP 800 steel shows a mixed microstructure composed by ferrite, bainite/martensite and retained austenite, as expected. The Le Pera reagent, used for TRIP steel, permit to highlight different phases with different colors. In particular, in Fig.2c, ferrite appears light brown, bainite appears dark brown, martensite and austenite appear white.

B. Mechanical Properties

Main mechanical properties, measured by tensile tests on smooth samples, are summarized in Table 3. The measured mechanical properties agree with the expected values for all the tested materials.

Fig.3 shows the engineering stress – strain curves obtained from smooth and notched tensile samples in the as-received conditions, without hydrogenation.

As expected, the mechanical behavior of the tested steels is rather different. Hot Stamping and Martensitic steels, that have a martensitic microstructure, show higher mechanical strength and lower ductility. On the contrary, TRIP 800 steel, characterized by a large strain hardening effect associated with the presence of austenite in its microstructure, has very high ductility and lower strength.

C. SSRT

[3] JEOL is a trademark of the Japan Electron Optics Ltd., Tokio.

Fig.4 shows the engineering stress-strain curves obtained for notched samples when charged with different hydrogen contents. The reported hydrogen concentrations are the average values between the witness samples (hydrogenated together with tensile samples) representative of the pre-tensile hydrogen concentration and the post-tensile samples measured by using a region close to the fracture surface. Since samples are notched the total elongation is short and thus also the total time of SSRT test. Thus, the measured differences between pre and post tensile test have been always less than 10 %. Only three curves for each steel are shown in Fig.4: one relative to the as-received (without hydrogen) sample, one for the sample with the maximum tested hydrogen concentration and another one for a medium level.
It can be easily observed that the hydrogen concentration ranges are different for different steels. This is because of the different hydrogen solubility in them and their uptake abilities, which are strictly dependent on the microstructure and the electrochemical properties of each steel.

In stress-strain diagram, hydrogen acts by reducing the extension of curve, without any (or with very poor) modification before the necking point. In the international scientific literature different sensitive parameters are used as indicator of hydrogen effect on steels, such as the fracture stress or the ductility (elongation or area) reduction [10,14,23,25]. This last parameter is better in case of ductile and low work-hardening steels, where the fracture stress does not sensitively change with hydrogen content changes. On the contrary, for ultra high strength steels the elongation to fracture is not an useful parameter because the hydrogen can induce a fracture in the elastic range, where the elongation of samples with different hydrogen content tends to show very similar values. Moreover, the presence of notch in tensile specimen further decrease the elongation to fracture sensitivity to HE. Thus, authors preferred to limit the analysis to fracture stress parameter.
Fig.5 shows the so-called Embrittlement Curve of each steel, i.e. the strength *vs* hydrogen concentration data. Strength values passes from values close to the as-received steel strength (for low hydrogen concentrations), to a lower plateau at higher hydrogen concentrations. This two plateau are separated by a marked transition region. It is worth noting that this behavior is common for all the steel grades, from ductile to high strength steels [22-24]. In order to interpolate the experimental data the following expression was used [23]:

$$N.UTS = a - b \cdot \arctan\frac{C_H - c}{d},$$

where *N.UTS* is the UTS of notched specimen. C_H is the hydrogen concentration and *a*, *b*, *c* and *d* are fitting parameters. In particular, the *c* parameter is related to the position of the inflection point (the middle of the transition region), *d* to the transition width, *a* and *b* parameters to the plateau values.

As shown in Fig.5, the use of the "arctangent" function permits to well reproduce the experimental data.
In order to identify the concentration at which value the steel is affected by hydrogen embrittlement, the *c* value has been chosen as *Hydrogen critical concentration*, C_{Hcr}.
In Fig.5 the hydrogen critical concentration values, $C_{Hcr,}$ related to each steel, are reported, along with the Embrittlement Index (EI) calculated as follows:

$$EI = \frac{N.UTS_{noH} - N.UTS_{\max H}}{N.UTS_{noH}} \times 100,$$

where $N.UTS_{noH}$ and $N.UTS_{maxH}$ are the fracture stress values of the uncharged sample and in correspondence of the maximum tested hydrogen concentration, respectively.
The Embrittlement Index is the percentage of *N.UTS* reduction measured at high hydrogen content, in the concentration range correspondent to the low strength plateau. It is an indication of the maximum hydrogen effect on steel strength.
Results reported in Fig.5 show that the maximum EI value is reached for the Hot Stamping steel (about 75%), whereas lower EI values (about 25 %) are measured for the other ones.

Concerning the hydrogen critical concentration for embrittlement, the lowest value was found for M 1400 steel (about 1 wppm), while the other steels show higher values. Critical hydrogen concentration of TRIP 800 steel is about 2,5 wppm, about 4 wppm for M 1200 and Hot Stamping steels.
The embrittlement curve for M 1400 steel exhibits a further reduction of *N.UTS* after the low strength plateau. This particular feature, related to a change in hydrogen damage modality, will be deeply discussed in section IV.

D. Hydrogen absorbed during painting process

Fig.6 shows the hydrogen concentration values measured from samples subjected to the real painting pre-treatment. The reported measurement values are the average values calculated from three different samples.

All samples show an absorbed hydrogen concentration lower than about 0,4 wppm. As clearly visible in Fig.6, collected data do not show any specific trend related to the coating layer wholeness or to the painting cycle step.

IV. DISCUSSION

In Table 4 the main data extracted from SSRT tests are summarized.

It is worthnoting that also using very similar electrochemical charging conditions the hydrogen concentration is very different from steel to steel. This feature mainly depends on different microstructural features. Also martensitic steels with similar strength (HS1500 and M1400) showed very different hydrogen uptake ability. This is probably due to their different production process. HS 1500 is produced by hot rolling process, while M1400 steel is produced by cold rolling process. Although similar martensitic microstructure, little differences on its fineness, hardening or chemical composition are able to induce heavy differences in hydrogen uptake ability. This is confirmed by all the performed tests, both for the electrochemical charging of SSRT specimens and for the hydrogen absorbed during painting, where HS 1500 steel showed final hydrogen concentration values much higher than M1400 and M1200 steels. Obviously, the presence of austenite phase in TRIP steel make difficult the comparison with other steels in terms of hydrogen diffusivity and solubility. These differences induce also high differences in the hydrogen concentration range where the decreasing of mechanical properties appears, as visible in Fig.5.
In order to highlight the main hydrogen embrittlement properties, the results of each tested steel will be discussed in the following.

A. Hot Stamping Steel

Although all steel grades can suffer hydrogen embrittlement [9], high strength steels are usually more prone to this problem. As expected, hot stamping steel, characterized by a completely martensitic microstructure and very high strength levels (*N.UTS* of about 1600 MPa) shows a very high Embrittlement Index. The degradation of mechanical properties is very marked, for example the strength of notched specimen with a hydrogen concentration of about 9 wppm is about 400 MPa, with a strength reduction of more than 75 %.
Strength reduction of hot stamping steels similar to that here presented have been already reported in literature [11,14]. Lee et al. reported UTS values of about 400 MPa for samples charged to 1,7 wppm [11]. The discrepancy in hydrogen content that have caused a similar EI in Lee et al. work and the present data can be explained considering the difference in electrochemical charging conditions. They charged 1.7 mm in thickness tensile samples for only 30 min, but this time, according to the hydrogen diffusion coefficient (D) value, is not enough to produce a homogeneous

hydrogen concentration inside the samples. Thus, close to the steel surface the hydrogen concentration could be much higher than in the center part. In the present work, D was calculated by using a Devanathan-Stackurski [18] electrochemical permeation apparatus, following the ASTM standard G 148 - 97 [26]. Its value was about $6 \cdot 10^{-7}$ cm^2/s. Using similar D values, for a 1,7 mm in thickness sample, a time of about 6 hours had been needed to reach uniform concentration across the specimen [17]. Finally, the low toughness of a completely martensitic steel causes the rupture of samples at the onset of subsurperficial cracks, even if the bulk material does have a hydrogen concentration much lower than the superficial one.
As shown in Fig.7a, the fractographic analysis showed ductile fracture for the as-received sample. Increasing the hydrogen content a typical hydrogen induced quasi-cleavage fracture appears (Fig.7b) with presence of some fine secondary cracks. At hydrogen concentration higher than the critical one, the secondary cracks enlarge and some intergranular component of primary crack can be highlighted, as visible in Fig.7c.

Post tensile samples have been sectioned in order to highlight the microstructural characteristic of the crack initiation sites. Fig.8 shows some of these on Hot Stamping steel sample charged with 5.2 wppm of hydrogen. Both transgranular and intergranular fractures have been found as shown in Fig.8a and Fig.8b, respectively. The analysis have not shown any particular correlation between the crack onset and the microstructural features of HS steel.

B. Martensitic steels

The embrittlement curve of M 1400 steel shows a critical concentration of about 1 wppm and an Embrittlement Index of about 25 %.
In order to highlight the main factor influencing the hydrogen embrittlement susceptibility of martensitic steels a deep microstructural analysis has been performed on longitudinal section of post tensile samples in regions close to the failure surface. A great part of hydrogen cracks have been found to start from inclusion particles. Micrograph in Fig.9 shows a typical hydrogen crack generated on an inclusion particle for a sample of M 1400 steel charged at 3.0 wppm of hydrogen. The dangerous shape factor of elongated inclusions can contribute to increase the hydrogen embrittlement susceptibility.

Performing EDX microanalysis on inclusions, they have resulted to be constituted mainly by Ca, Si, Al and Ti particles.
Fig.10 shows the fracture surface for M 1400 samples with different hydrogen contents. The uncharged sample (see Fig.10a) presents a ductile fracture, while hydrogenated samples are subjected to brittle fracture. For hydrogen concentration lower than about 2 wppm samples have shown a mixed transganular – intergranular fracture (see Fig.10b for a 1.2 wppm charged sample), while, for higher hydrogen content there has been a predominance of intergranular fracture, as shown in Fig.10c for a sample charged at 3.0wppm, as expected for the increasing of hydrogen activity [27].

After the high concentration plateau a further decreasing of strength level is clearly visible for M1400 steel, showed in Fig.5b as hollow points. Post tensile fractographic analysis (see Fig.11) showed that at hydrogen concentration higher than about 3 wppm the fracture surface changes appearance .
For lower hydrogen concentration the low magnification fracture appearance is that typical of notched samples with a triangular area close to the notch associated with the stress intensification region (see Fig.11a to Fig.11c). For higher concentration, this morphology has disappeared and the fracture surface is composed by several elliptical cracks (see Fig.11d). Deep secondary cracks are also clearly visible. This behavior has been probably due to the formation of hydrogen induced cracks during the electrochemical charging, that greatly lower the samples strength. The failure of a

sample with a concentration of about 4 wppm during electrochemical charging confirm the abovementioned explanation. The dispersion of strength values for samples with more than 3 wppm is suggested to be related to the stochastic mechanism that drives the crack formation and to the crack length presents after hydrogenation, before to be tensile tested. Authors have decided to not include these data in the embrittlement curve fitting, since this curve is valid for stress assisted hydrogen embrittlement.

In the present explored experimental conditions, hydrogen induced cracks generated during electrochemical charging have been found only for the M 1400 steels, although authors can not exclude the possibility to induce hydrogen cracking on others steels at much higher hydrogen concentrations.
M 1200 steel shows an embrittlement curve similar to M 1400 steel. The lower strength level determines a lower hydrogen embrittlement susceptibility, shifting the hydrogen critical concentration to higher values (about 4 wppm).
Concerning the general hydrogen embrittlement behavior of very high strength steels (with strength level higher than 1200 MPa) could be important to highlight the role of stamping modalities.
The hydrogen embrittlement susceptibility of high grade martensitic steels could be increased by the fact that auto body components are produced by cold stamping process that gives high residual stresses due to springback effect [28]. Although the hot stamping steel (comparable in terms of strength and ductility) has a much higher Embrittlement Index the almost completely absence of residual stresses derived by the hot stamping process can play favorably on its hydrogen embrittlement susceptibility.

C. TRIP steel

The presence of austenite deeply influences the hydrogen behavior in steel. Thanks to the very high solubility and low diffusivity of hydrogen in it, austenite acts as a sink for hydrogen, lowering its mobility and increasing the final hydrogen concentration. Thus, in TRIP steel the hydrogen concentration in austenite is much higher than in the other phase.
During the deformation of TRIP steels, austenite transform into martensite (TRIP effect), which is the microstructure the most susceptible to hydrogen embrittlement. Thus, it is fair to say that just after the application of stress the hydrogen enriched transformed martensite quickly cracks, inducing the failure of specimen. Moreover, the not stable austenite of TRIP steels could be more and more unstabilized by the presence of hydrogen, as happens for austenitic stainless steels where hydrogen can induce martensitic transformation and related failure (see for example [29]). Probably, this is the reason because the embrittlement curve of TRIP 800 steel does not present a marked plateau in the low concentration region, as clearly visible in Fig.5.
The microstructural examination of post tensile samples electrochemically charged with hydrogen, have shown the presence of crack onsets in correspondence of the hard particles, as shown for example in Fig.12. This result is in agreement with the above suggested fracture mechanism. Moreover, other researches highlighted similar crack initiation mechanisms. Using EBSD techniques Imlau et al. [26] found a high correlation between the region where cracks form and martensite transformation areas. Moreover, Ronevich et al. [14] found some cracks starting from hard particles (martensite islands) and propagating into ferrite grains.

Fractographic analysis have shown that fracture surfaces become more and more brittle by increasing the hydrogen content, as shown in Fig.13. The uncharged sample presents a completely ductile fracture (Fig.13a). Increasing the hydrogen content the brittle percentage of fracture surface increases, above all for concentration higher than the critical one (Fig.13b to 13d).

Moreover, it is important to note that the ductile microstructure of TRIP 800 steel and the low tested grade (comparing to the other tested steels) limit the strength reduction in presence of high hydrogen concentration to about 25 %.
Despite of the presence of austenitic phase that is usually considered to have higher hydrogen embrittlement resistance thanks to its higher toughness and its lower hydrogen diffusivity, TRIP 800 steel shows some susceptibility to hydrogen embrittlement in respect to its low grade. The high hydrogen uptake ability due to the austenite presence along with its tendency to transform into a hydrogen rich martensitic phase, impose particular care in the use of this steel as structural material when high hydrogen uptake conditions could be present.

D. Hydrogen Absorbed during Body In White painting process

The hydrogen critical concentrations measured by SSRT tests are not an exhaustive expression of the hydrogen embrittlement susceptibility of a steel. This value has to be correlated to the hydrogen concentration absorbed in the real conditions, during the production process or service life of the steel components.
The measurement of hydrogen content absorbed during the painting pre-treatment processes of Body In White have been performed on industrial plant during a real treatment. In this way, the coupons of the analyzed steels have exactly followed the same process of real cars. As already detailed, two types of samples have been used, one with the coating layer undamaged, and another one with scratches, in order to simulate damage on the coating layer.
As reported in Fig.6, the measured hydrogen contents have been always less than 0.4 wppm in all the tested conditions (after phosphatizing, after EDP and after EDP curing line steps). This means that for all the tested steels the absorbed hydrogen is much lower than the hydrogen critical concentration. Hot Stamping and TRIP 800 steels showed the highest values of absorbed hydrogen, while martensitic steels showed lower tendency to be hydrogenated. Concerning TRIP 800 steel, its hydrogen uptake ability derived above all by the austenitic phase present in the microstructure.
The measured hydrogen concentrations show the same differences observed during electrochemical charging of tensile samples, being much higher for Hot Stamping and TRIP 800 steels than martensitic steels, highlighting a different hydrogen uptake ability.
No trend is visible either in function of the steel grade, or of the cycle steps.
Considering the highest hydrogen concentration measured for each steel and using the interpolation formula of the embrittlement curve it is possible to calculate the strength of materials after the painting process. The strength reduction is less than 1% for all the tested steels. Thus, *de facto*, they do not suffer hydrogen embrittlement after the BIW production process.
Moreover, since BIW is mainly assembled using cold formed components, some coupons of the analyzed steels have been bended up to reach the 80% of the ultimate real stress.
In order to analyze their hydrogen delayed cracking susceptibility during painting, these coupons followed the same painting line as for the measurement of absorbed hydrogen. Then bended samples were taken into observation for two weeks in order to register the time to eventual cracks formation. The time of two week is much higher than that needed to make zero the hydrogen concentration in the coupon (that, thanks to the short time of process, was able to absorb hydrogen only in the surface). No cracks have been found in all of the tested steels, thus confirming the absence of hydrogen embrittlement associated to the autobody production process. Nevertheless, further investigations will be performed in order to highlight the possible hydrogen uptake during the car service life.

V. CONCLUSIONS

From the above mentioned tests performed on AHSS it is possible to highlight the following conclusions:

- Hot stamping steel has shown a heavy reduction of tensile strength (more than 75%) for hydrogen concentration of about 7 wppm. As expected, its fully martensitic microstructure is highly susceptible to hydrogen embrittlement.
- Martensitic steels with very high tensile strength have shown a hydrogen critical concentration of about 1 and 4 wppm for M 1400 and M 1200 steels, respectively. In the analysis of crack initiation sites, a predominance of hydrogen induced defects in correspondence of inclusion particles has been found. These defects can contribute to the hydrogen embrittlement susceptibility of this steel class. Moreover, M 1400 steel have demonstrated a high hydrogen induced cracking susceptibility at hydrogen concentration higher than about 3 wppm, with the formation of cracks during the electrochemical charging. M 1200 steel, thanks to its lower resistance, has a higher hydrogen critical concentration, and it does not show tendency to crack in absence of external stresses.
- Although the presence of austenitic phase in its microstructure, the analyzed TRIP 800 steel has shown some susceptibility to hydrogen embrittlement. Its hydrogen critical concentration is about 2,5 wppm. This behavior has been correlated to the presence of austenite that transforms into martensite during deformation. The high hydrogen solubility in this phase can increase the tendency to transform and can produce a hydrogen rich martensitic phase that quickly cracks during straining.
- The hydrogen concentration absorbed during the pre-treatment of painting cycle have shown values much lower than the critical concentrations in all the analyzed conditions. Moreover, no hydrogen induced delayed cracks have been found on bended region of the same samples. These results suggest that the tested AHSS can be used to build BIW components with a good safety factor.

REFERENCES

1. International Iron & Steel Institute Committee on Automotive: “Advanced high strength steel (AHSS) application guidelines Version 3”, 2006, online at www.worldautosteel.org.
2. C. Federici, S. Maggi, S. Rigoni: Proc. Conf. on New Developments on Metallurgy and Applications of High Strength Steels, Buenos Aires, May 26-28, 2008.
3. Y. Mukai: Kobelco Tech. Rev., 2005, n.26, pp. 26-31.
4. B.C. De Cooman, L. Chen, H.S. Kim, Y. Estrin, S.K. Kim, H. Voswinckel: Proc. Conf. on New Developments on Metallurgy and Applications of High Strength Steels, Buenos Aires, May 26-28, 2008.
5. W. Bleck, K. Phiu-On: Mater. Sci. Forum, 2005, Vol.500/501, pp. 97-114.
6. R.A. Oriani, J.P. Hirth, M. Smialowski: Hydrogen degradation of Ferrous Alloys, Noyes Publications, Park Ridge, NJ, USA, 1985.
7. J.P. Hirth: Metall. Trans. A, 1980, Vol.11A, pp. 861-890.
8. ASM Materials Handbook, Metals Handbook, 9th edn., vol. 13, Corrosion, ASM International, Materials Park, OH (1987), p.330.

9. I.M. Bernstein: Hydrogen Effect in Materials, Proceedings of the 5th International Conference on the Effect of Hydrogen on the Behavior of Materials, Ed. By A.W. Thompson and N.R. Moody, TMS publication, 1996, pp. 3-11.
10. T.B. Hilditch, S-B. Lee, J.G. Speer, D.K. Matlock: SAE SP n. 1764, 2003, pp. 47-56.
11. S-J. Lee, J.A. Ronevich, G. Krauss, D. Matlock: ISIJ Int., 2010, vol.50, n.2, pp. 294-301.
12. K.H. So, J.S. Kim, Y.S. Chun, K.T. Park, Y-K. Lee, C.S. Lee: ISIJ Int., 2009, vol.49, n.12, pp. 1952-1959.
13. H. Mohrbacher: Mater. Sci. and Tech. (MS&T), Proc. Conf. on Steel Product Metallurgy and Application, October 5-9, Pennsylvania (USA), 2008.
14. J.A. Ronevich, J.G. Speer, D.K. Matlock: SAE Int. J. Mater. Manuf., 2010, vol.3 (1), pp. 255-267.
15. W.J. Pollock: ASTM-STP 962 "Hydrogen Embrittlement: Prevention and Control", L. Raymond, Editor, American Society for Testing and Materials (ASTM) STP 962 (1988), Philadelphia USA, pp. 68-80.
16. I. Krylova: Progress in Organic Coatings, 2001, vol.42, pp. 119–131.
17. J. Cranck: The Mathematics of Diffusion, 2nd edition, Oxford Science Publications, 1975, pp. 49-51.
18. M.A.V. Devanathan, Z. Stachurski: Proc. R. Soc. London, Ser. A, 1962, 270 (1340), pp. 90-102.
19. ASTM G129 – 00 (reapproved 2006): Standard Practice for Slow Strain Rate Testing to evaluate the Susceptibility of Metallic Materials to Environmentally Assisted Cracking, ASTM International, West Conshohoken, PA, USA, 2006.
20. D.A. Berman, V.S. Agarwala: ASTM-STP 962 "Hydrogen Embrittlement: Prevention and Control", L. Raymond, Editor, American Society for Testing and Materials (ASTM) STP 962 (1988), Philadelphia USA, pp. 98-104.

21. ASTM F 1113 – 87 (reapproved 2005): Standard test method for Electrochemical measurement of diffusible hydrogen in steels (Barnacle electrode), ASTM International, West Conshohoken, PA, USA, 2005.

22. R. Valentini, A. Solina, S. Matera, P. De Gregorio: Metall. Mater. Trans. A, 1996, Vol.27A, pp. 3773-3780.

23. M. Beghini, G. Benamati, L. Bertini, I. Ricapito, R. Valentini: J. Nucl. Mater., 2001, Vol.288, pp. 1-6.

24. G. Lovicu, M. De Sanctis, A. Dimatteo, R. Valentini, P. Trombetti: 32° Convegno Nazionale AIM, September 24-26, Ferrara, ITALY, 2008.

25. E. Akiyama, S. Li, Z. Zhang, M. Wang, K. Matsukado, K. Tsuzaki, B. Zhang: Effect of Hydrogen on Materials, Proceedings of the 2008 International Hydrogen Conference, B. Somerday, P. Sofronis, R. Jones ed., ASM International Materials Park, OH, 2009, p.54-61.

26. ASTM standard G 148 -97 (reapproved 2003): Standard Practice for Evaluation of Hydrogen Uptake, Permeation, and Transport in Metals by an Electrochemical Technique, ASTM International, West Conshohoken, PA, USA, 2003.

27. C.J. McMahon, X. Liu, J. Kameda, M.J. Morgan: Effect of Hydrogen on Materials, Proceedings of the 2008 International Hydrogen Conference, B. Somerday, P. Sofronis, R. Jones Editors, 2009, ASM International, Materials Park, Ohio, pp.46-53.

28. Die Design Handbook, Society of Manufacturing Engineers (SME), Dearborn Michigan, 1990, pp. 6-7 – 6-9.

29. S.M. Teus, V.N. Shyvanyuk, V.G. Gavriljuk: Mat. Sci. Eng. A, 2008, 497, pp.290-294.

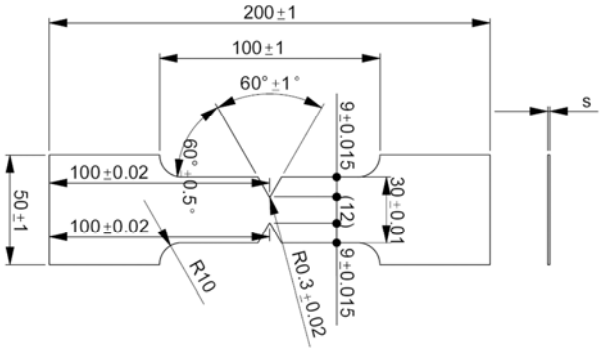

Fig.1: Specimen geometry and dimensions for SSRT tests. The thickness *s* depends on the steel strip thickness.

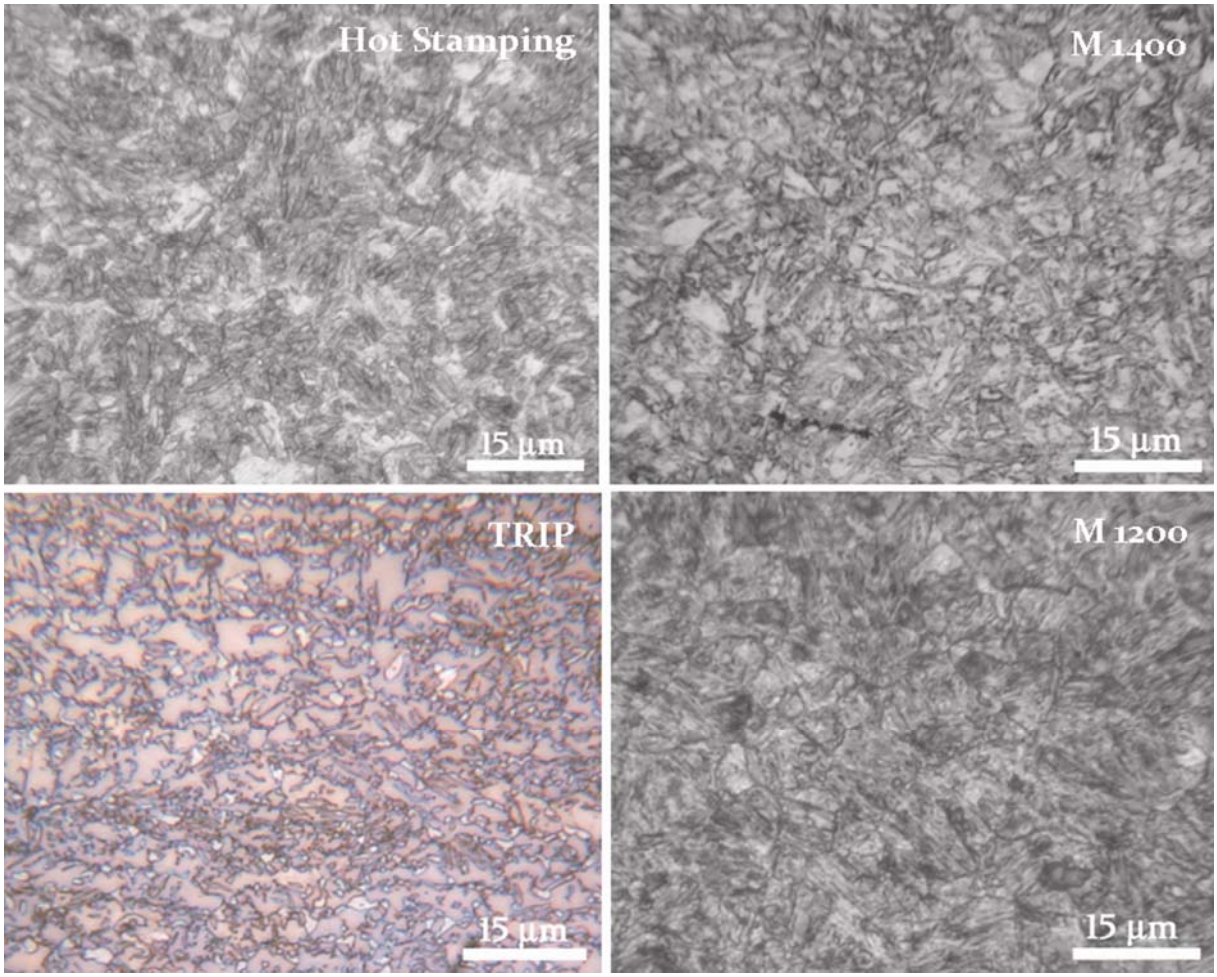

Fig.2: Microstructures of tested Advanced High Strength Steels. A) Hot stamping steel (Nital reagent); b) M 1400 steel (Nital reagent); c) TRIP 800 steel (Le Pera etchant): ferrite in light brown, bainite in dark brown, martensite and austenite in white; d) M 1200 steel (Nital reagent).

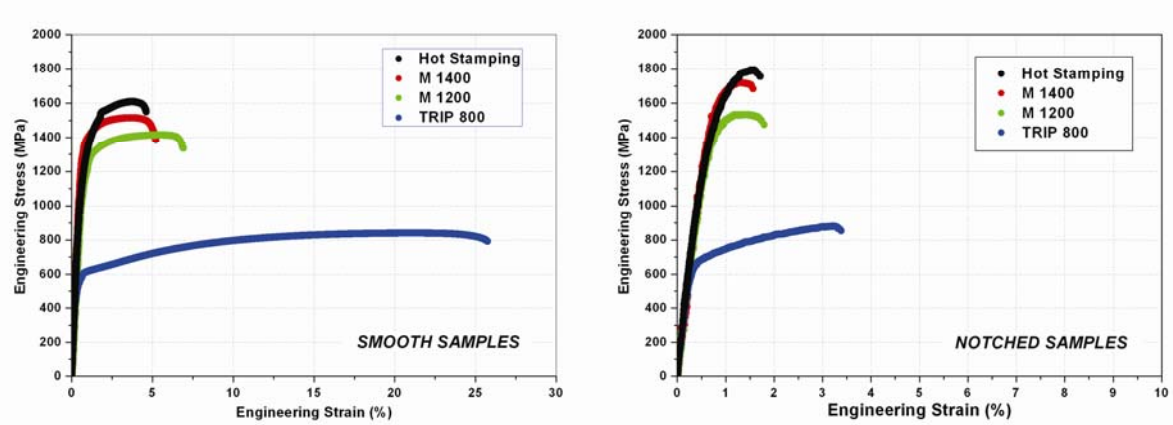

Fig.3: Engineering stress-strain curves for the tested AHSS in the as-received (hydrogen uncharged) conditions. a): Stress – strain curve for smooth samples; b): Stress – strain curve for notched samples.

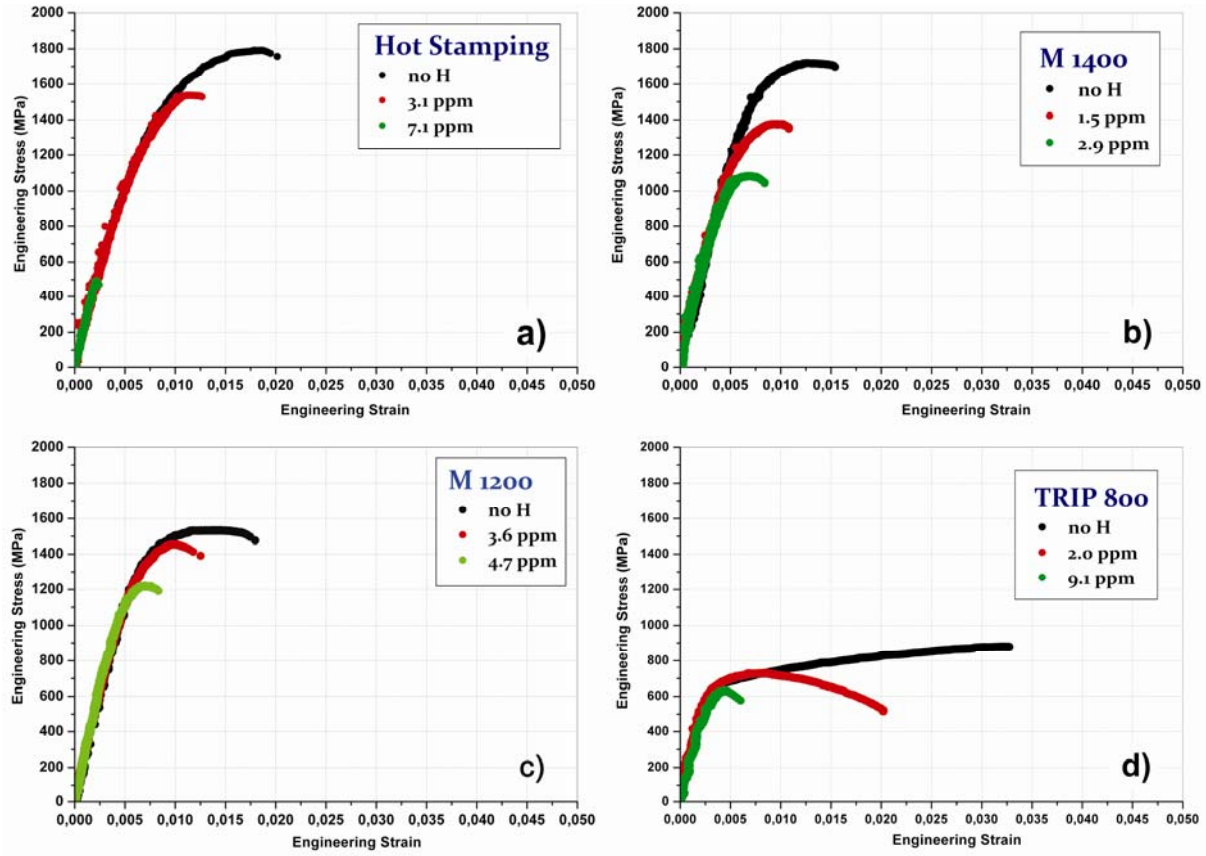

Fig.4: Stress-Strain curves of tested steels electrochemically charged at different hydrogen contents. A): Hot Stamping steel; b): M 1400 steel; c): M 1200 steel; d): TRIP 800 steel.

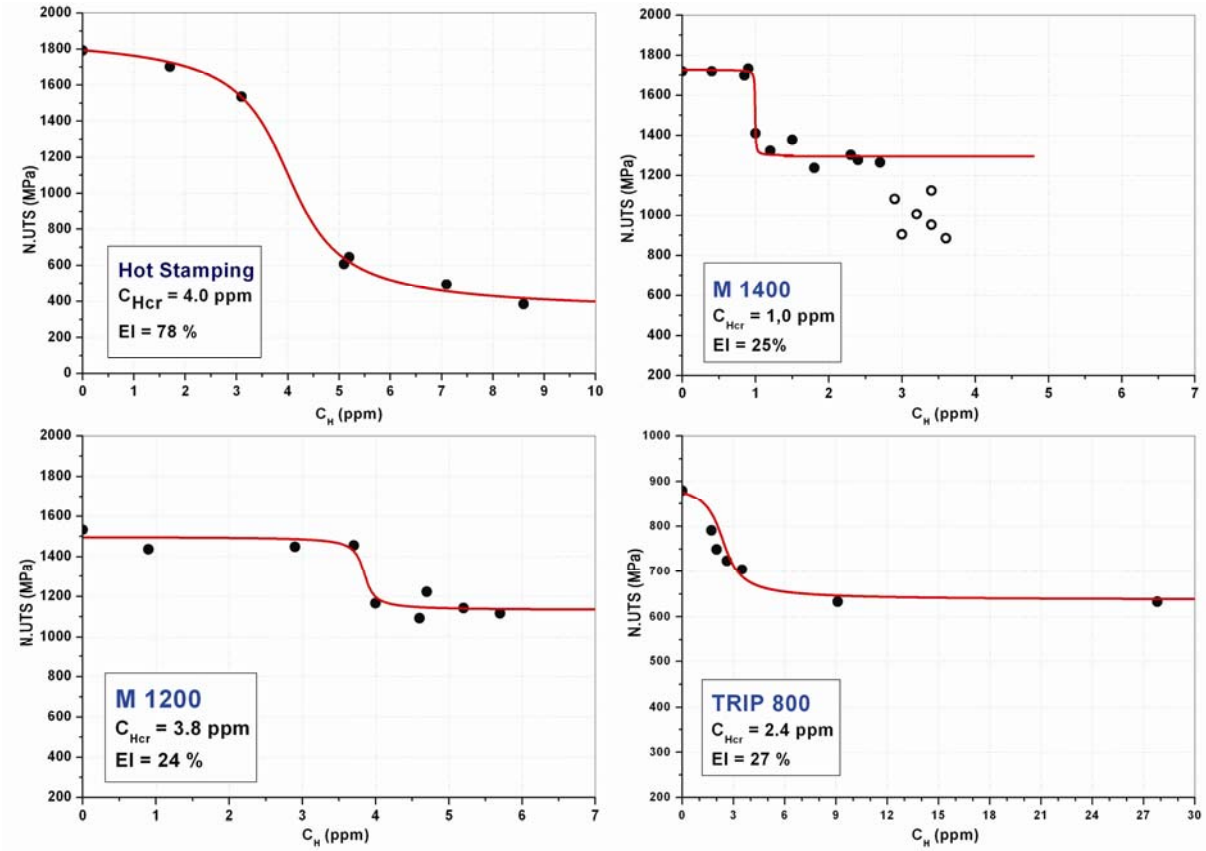

Fig.5: Hydrogen embrittlement curves of tested steels. a) Hot Stamping steel; b) M 1400 steel; c) M 1200 steel; d) TRIP 800 steel. For each steel the hydrogen critical concentration for embrittlement and the embrittlement index are reported. Some of the M1400 steel data are shown as hollow point in order to differentiate them in respect to the others. The meaning of this difference is described in text (detailed in IV.B section). N.UTS is the UTS measured for notched specimen.

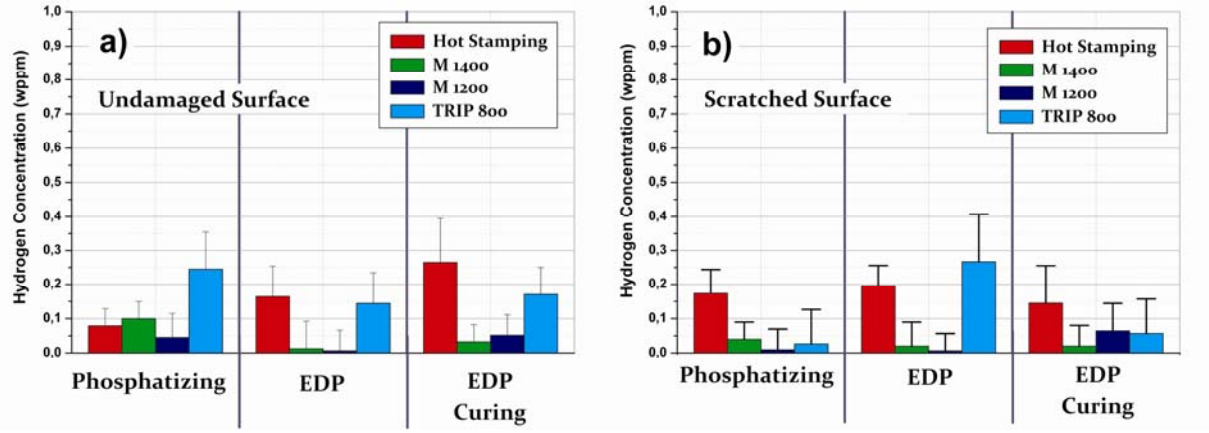

Fig.6: Hydrogen concentration, measured by the electrochemical Barnacle method, absorbed during the following painting line steps: phosphatizing, electrodeposition painting and final curing.
a) results for undamaged surface; b) results for scratched surface.

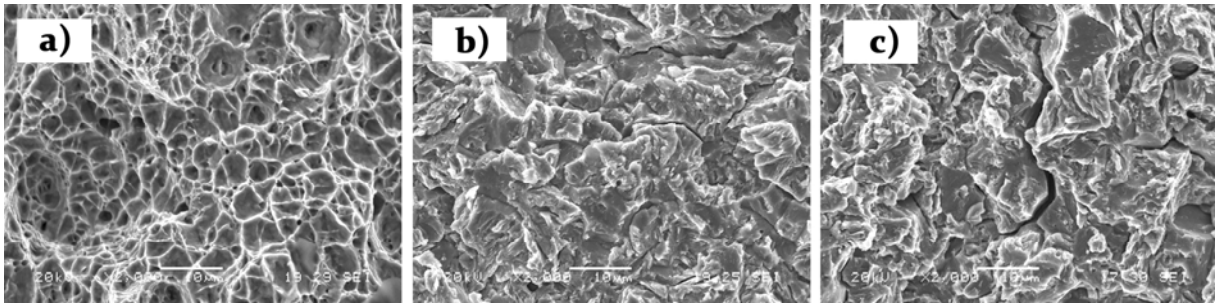

Fig.7: Micrographs of fracture surface of Hot Stamping Steel samples charged with different hydrogen contents. A): uncharged specimen; b): sample electrochemically charged at 2.6 wppm; c): sample electrochemically charged at 7.1 wppm.

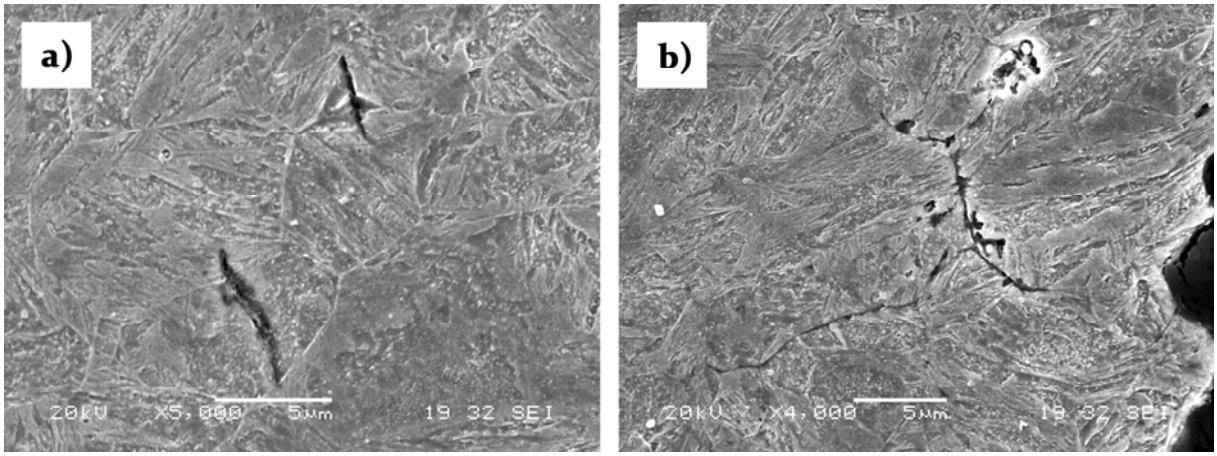

Fig.8: Micrographs showing the longitudinal section of post tensile Hot Stamping steel sample (with 5.2 wppm) in the region close to the fracture surface. a): transganular cracks; b): intergranular cracks.

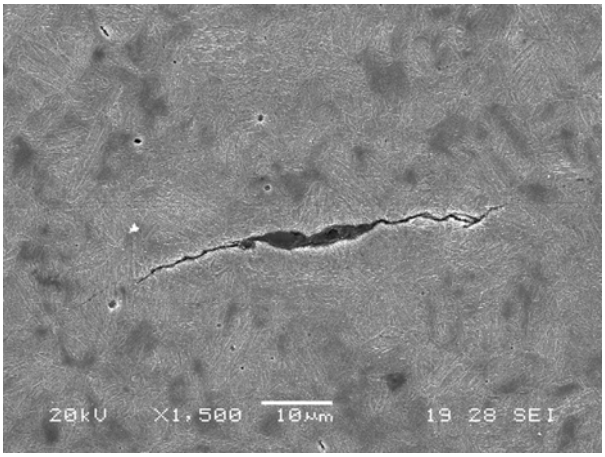

Fig.9: Example of hydrogen induced crack started from an inclusion particle, in a M 1400 steel electrochemically charged at 2.7 wppm.

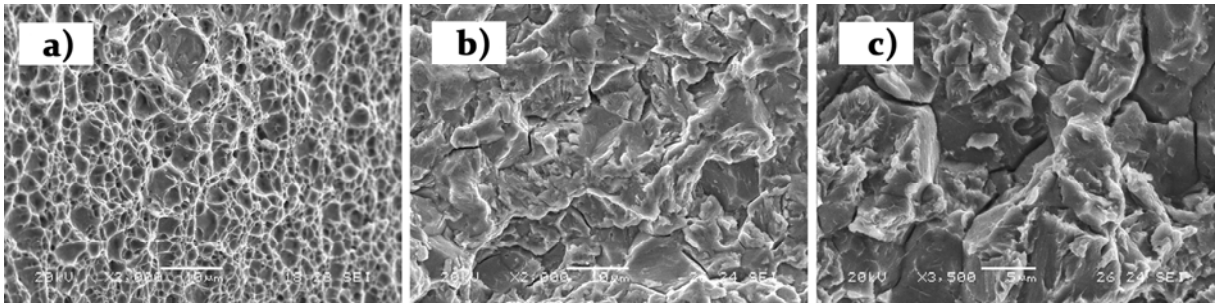

Fig.10: Micrographs of fracture surface of M 1400 steel samples charged with different hydrogen contents. A): uncharged specimen; b): sample electrochemically charged at 1.2 wppm; c): sample electrochemically charged at 2.7 wppm.

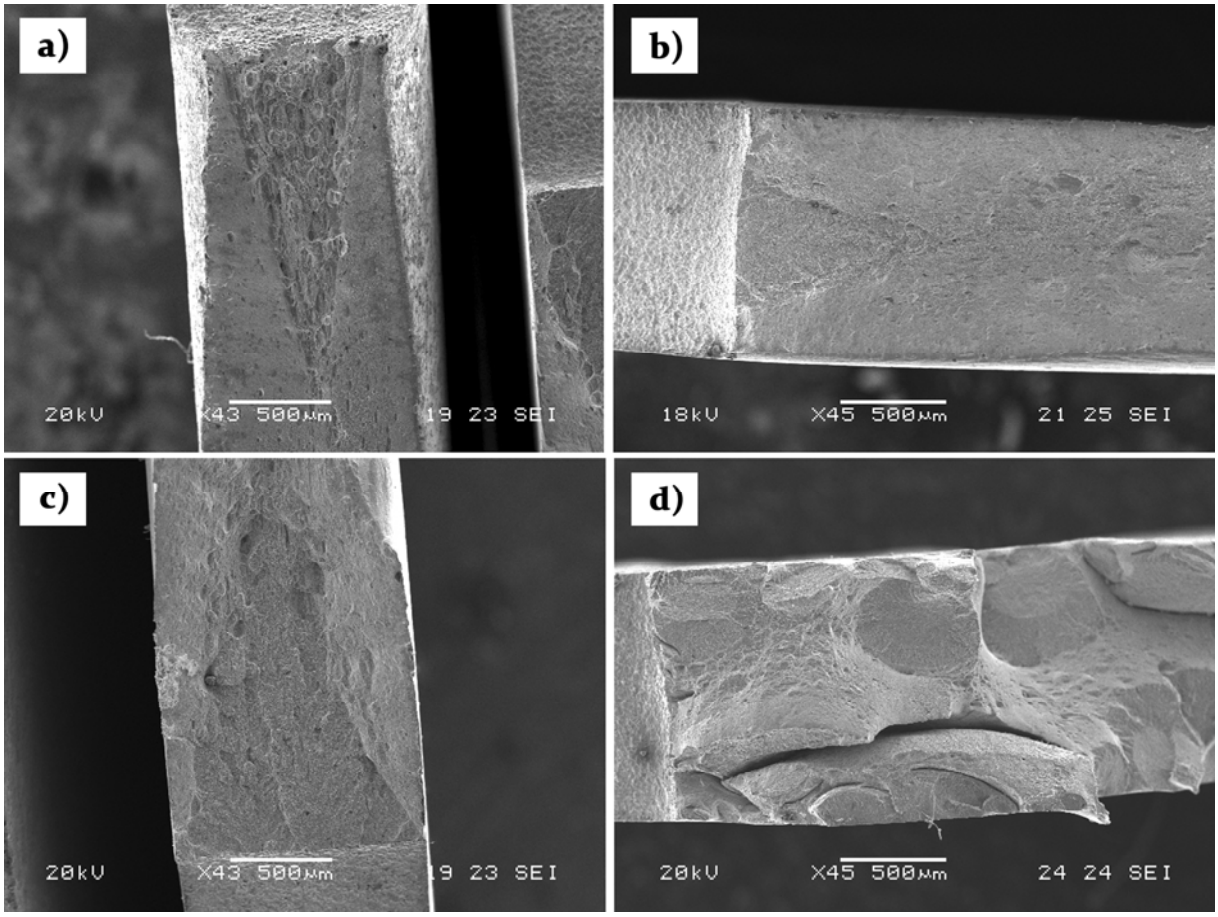

Fig.11: SEM micrographs showing the fracture surface of M 1400 post tensile samples with different hydrogen contents. A): uncharged specimen; b): 0.9 wppm; c): 2.3 wppm; d): 3.4 wppm.

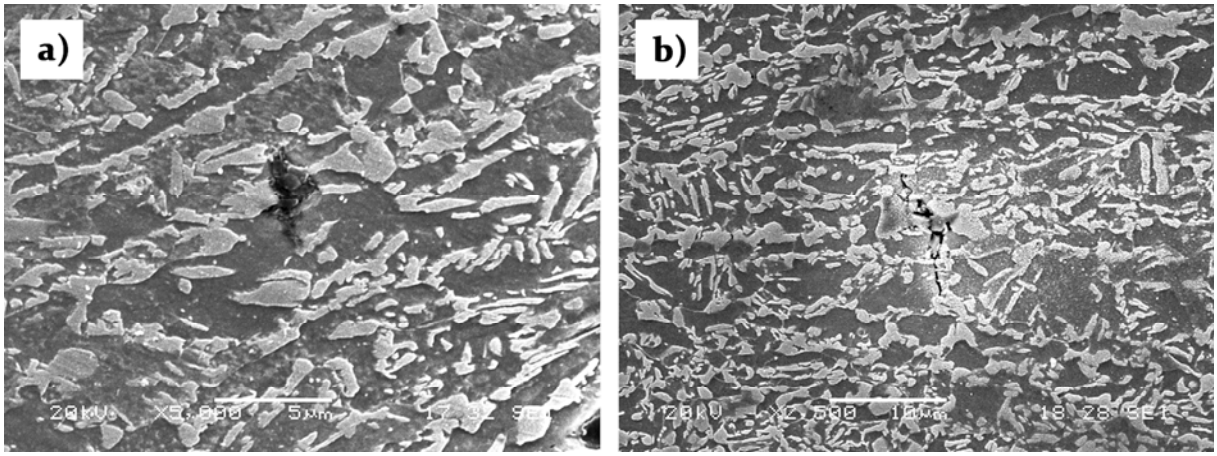

Fig.12: Micrographs showing the longitudinal section of post tensile TRIP 800 steel sample with different hydrogen contents in the region close to the fracture surface. a): 3.5 wppm; b): 28 wppm.

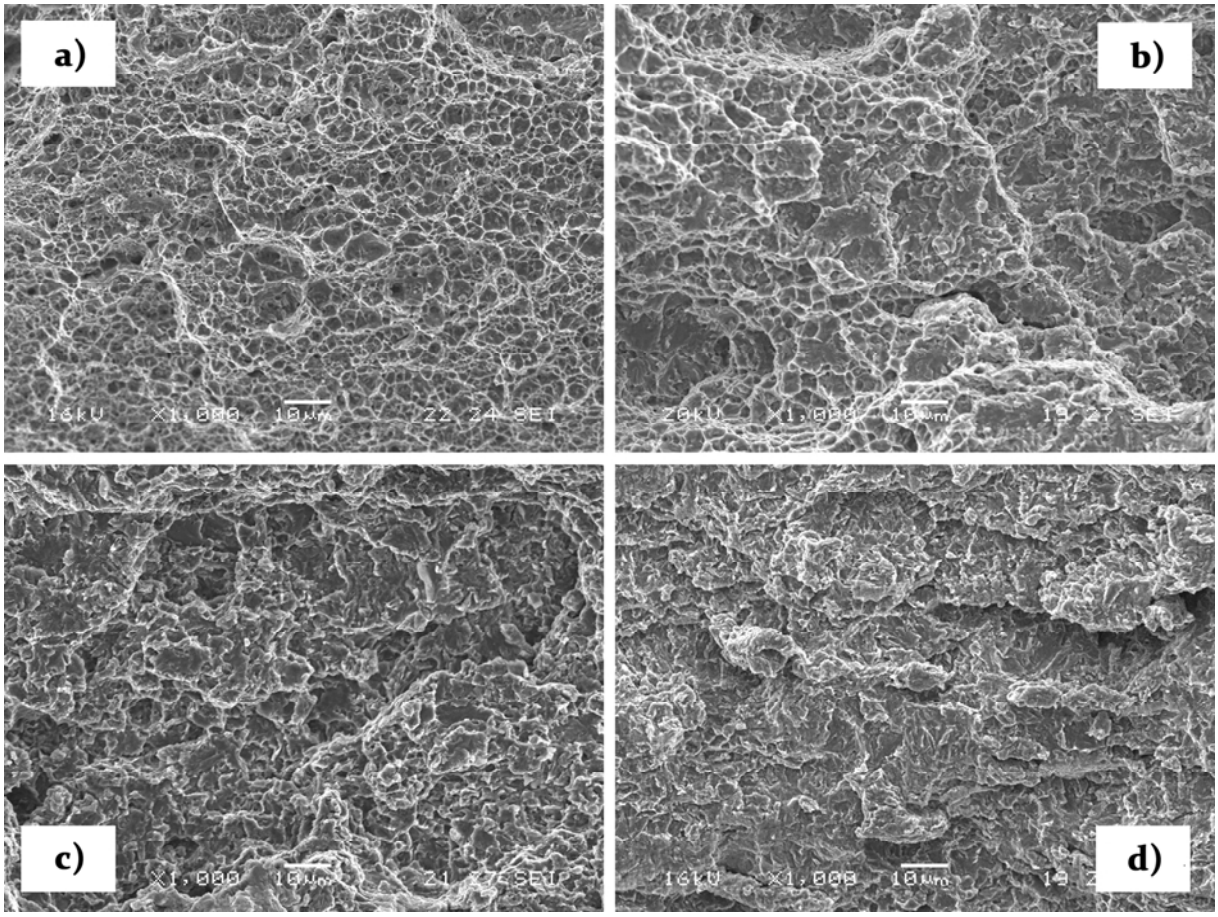

Fig.13: Micrographs of fracture surface of TRIP 800 steel samples charged with different hydrogen contents. a): uncharged specimen; b): sample electrochemically charged at 3.5 wppm; c): sample electrochemically charged at 9.1 wppm; d): sample electrochemically charged at 28 wppm.

Table 1: Thickness, coating type and chemical composition of tested steels.

Steel	Thickness (mm)	Coating type	Chemical Composition						
			%C	%Mn	%Si	%Cr	%Ti	%Al	B (wppm)
HS 1500	1.80	Al-Si	0,22	1,25	0,25	0,22	0,04	0,04	> 20
M 1400	1.25	Electrogalv	0,18	1,51	0,35	0,21	0,04	0,05	> 20
M 1200	2.00	Electrogalv	0,12	1,70	0,21	0,03	0,03	0,04	> 20
TRIP 800	1.12	Galv	0,19	2,12	0,63	0,03	0,01	1,02	-

Table 2: Main pre-treatment painting process parameters registered during the cycles used for the hydrogen absorption analysis.

Phosphatizing	T = 50 °C	pH = 4.7
Primer Electrodeposition	V = 220 ÷ 310 V	pH = 6
EDP Curing	T = 170 ÷ 190 °C	

Table3: Mechanical properties of the analyzed steels in the as-received conditions.

	UTS (MPa)	YS (MPa)	Elong. (%)
HS 1500	1615	1550	6
M 1400	1520	1410	5
M 1200	1305	1205	9
TRIP 800	815	620	26

Table 4: Hydrogen concentrations and tensile properties measured in function of electrochemical charging for all the tested steels.

Steels	Parameters	Charging Conditions		
		Low[1]	High[2]	Very High[3]
HS 1500	C (ppm)	1.8 ÷ 5.2	5.1 ÷ 8.6	
	N.UTS Red.[4] (%)	5 ÷ 65	65 ÷ 78	
	El.. Red.[5] (%)	10 ÷ 55	75 ÷ 90	
M 1400	C (ppm)	0.4 ÷ 1.8	1.5 ÷ 3.3	2.5 ÷ 3.6
	N.UTS Red.[4] (%)	0 ÷ 25	20 ÷ 42	25 ÷ 48
	El.. Red.[5] (%)	10 ÷ 15	35 ÷ 50	35 ÷ 60
M 1200	C (ppm)	0.9 ÷ 4.7	4.0 ÷ 5.8	
	N.UTS Red.[4] (%)	5 ÷ 28	23 ÷ 25	
	El.. Red.[5] (%)	0 ÷ 55	35 ÷ 65	
TRIP 800	C (ppm)	1.7 ÷ 3.5	2.6 ÷ 27.8	
	N.UTS Red.[4] (%)	10 ÷ 20	17 ÷ 27	
	El.. Red.[5] (%)	0 ÷ 75	40 ÷ 85	

[1] (Low): NaOH 0,1 N + As_2O_3 25 mg/l with current density between 1 and 10 mA/cm^2;
[2] (High): H_2SO_4 0,1 N + As_2O_3 25 mg/l with current density between 1 and 50 mA/cm^2;
[3] (Very High): H_2SO_4 1 N + $NaAsO_2$ $5 \cdot 10^{-4}$ N with current density between 10 and 50 mA/cm^2;
[4]: N.UTS Red. = Reduction of Notched Ultimate Tensile Strength in respect to uncharged sample.
5: El. Red. = Reduction of Elongation to Fracture in respect to uncharged sample.